Chapter 44
Cement Failure Caused by Thermal Stresses with Casing Eccentricity During CO_2 Injection

Xuelin Dong, Deli Gao and Zhiyin Duan

Abstract Carbon capture and sequestration (CCS) is one of the most promising technologies to mitigate greenhouse gas levels. To ensure an effective underground storage, well integrity is critical to isolating the injected fluid between different zones or back to the surface. Among the wellbore components, the cement sheath is the most important sealing element for zonal isolation. However, cement is vulnerable and prone to cracking that may provide leakage pathways for CO_2. Both laboratory study and field test show that thermal stresses caused by the temperature variation in the wellbore are a major factor for the mechanical integrity loss of cement. This work focuses on the mechanical response of the casing-cement-formation section above the injection zone. We firstly propose a wellbore flow model to predict the temperature distribution along the well depth. Then we calculate the induced stress in cement during injection by a finite element simulation. To identify the cement failure mode, we introduce failure factors by the Mogi-Coulomb criterion, tensile strength and interfacial strength corresponding to shear compressive failure, radial cracking and debonding at the casing/cement or cement/formation interfaces, respectively. A parametric study is conducted to investigate the influence of the injection temperature and rate as well as casing eccentricity on failure factors. The results show that radical cracking and debonding at the cement/formation interface are the main failure modes during CO_2 injection. Both the two failure factors would increase linearly as the injection temperature decreases while they grow non-linearly with the injection rate. In addition, the casing eccentricity exacerbates the risk of cement integrity loss by increasing failure factors. This study provides a failure assessment of CO_2 geological sequestration and guidelines for injection operations.

Keywords Well integrity · Thermal stress · Failure mode

X. Dong (✉) · D. Gao
Key Laboratory of Petroleum Engineering, China University of Petroleum, Beijing 102249, China
e-mail: dongxl@cup.edu.cn

Z. Duan
Beijing Key Lab of Heating, Gas Supply, Ventilating and Air Conditioning Engineering, Beijing University of Civil Engineering and Architecture, Beijing 100044, China

H. Okada and S. N. Atluri (eds.), *Computational and Experimental Simulations in Engineering*, Mechanisms and Machine Science 75,
https://doi.org/10.1007/978-3-030-27053-7_44

44.1 Introduction

Carbon capture and sequestration (CCS) has been recognized as an attractive technology to mitigate greenhouse gas levels in the world [1, 2]. Injecting large tonnages of CO_2 into saline aquifers or depleted oil and gas reservoirs through wells onshore or offshore is an effective method of long-term storage [3]. Although several research, pilot or even commercial CO_2 storage projects have been successfully implemented, there are still concerns on their safety among scientists, engineers and publics [4]. Leakage of the stored CO_2 or re-emerging to the surface is one of the most concerned issues. Therefore, maintaining the well integrity to prevent leakages is crucial to a long-term storage.

CO_2 injection and storage pose various challenges to well integrity. The injected cold fluid would induce complex geochemical and geomechanical interactions between barrier materials, reservoir formation and underground fluids [5, 6]. Damages to barrier materials, especially to the cement sheath would cause embedded cracks or interfacial debonding, which provide potential pathways for CO_2 leakage. Both laboratory experiments and field tests have demonstrated that the temperature fluctuation caused by the temperature difference between the cold injected fluid and hot formation is a primary factor to induce large thermal stresses in cement [7–9]. The induced stress once surpasses the material's strength, cement failure will occur. Hence, a proper estimation of thermal stress in cement is valuable to evaluate the cement integrity.

Many researchers have studied thermal stresses in injection wells using analytical or numerical methods. Thiercelin et al. [10] proposed an analytical mechanical model based on linear elastic theory to investigate the role of thermal perturbations on the mechanical response of the cement. They showed that cement failure could be avoided by selecting proper thermo-elastic properties of wellbore materials. Yu et al. [11] carried out coupled thermo-poromechanical multi-phase simulations to study the effect of thermal stresses on the caprock integrity. They concluded that injecting CO_2 at the temperature close to the aquifer significantly reduces the risk of caprock fracturing. Nygaard et al. [12] evaluated the integrity of CO_2 injection well by a 3D finite-element model, in which the cement and formation are treated as poroelastoplastic materials. They suggested that lower Young's modulus and Poisson's ratio of the cement would reduce the risk of debonding and tensile failure. Aursand et al. [13] proposed a coupled flow and heat conduction model to determine injection parameters' effect on temperature variations in wells. Particularly, they showed that longer pauses between injections will induce a larger thermal stress which is enough to cause debonding at the casing/cement interface. Roy et al. [14] considered the initial damage in the cement and studied the impact of thermal stresses on cracking through stress intensity factors. They found that the existence of in-situ horizontal stresses has a positive effect on preventing damage evolution in cement.

This paper firstly presents a wellbore flow model that is used to provide the temperature profile along the well depth. Then we construct a mechanical model

based on thermoelastic theory to estimate the stress components in a casing-cement-formation section above the injection zone. Failure factors are defined to identify the failure modes according to material strength criteria. Finally, we estimate failure factors under different injection operations and investigate the effect of the casing eccentricity.

44.2 Wellbore Flow Model

Studies for well integrity of CO_2 storage have indicated that the temperature difference between the cold injected CO_2 and the hot surrounding rock will cause large thermal stresses in barrier materials. In particular, once the induced stress in cement exceeds its strength, damages or interfacial debonding would occur to undermine the well integrity. To estimate the stress in cement during CO_2 injection, it is of great importance to obtain the temperature profile along the well. This can be achieved by wellbore flow models.

Numerous models have been proposed to investigate the flowing temperature and pressure during CO_2 injection [15]. These models intend to describe CO_2 wellbore flow and heat transfer in different working conditions including single-phase flow and two-phase flow [16]. In this study, we assume that the injected CO_2 is in a liquid state. Industry practices suggest injecting liquid CO_2 that is more efficient due to its higher density than its supercritical gaseous counterpart. In addition, we suppose the flow along the well depth is steady while the radial heat transfer is unsteady as illustrated in Fig. 44.1. Hence, the governing equations for wellbore flow are presented as [17].

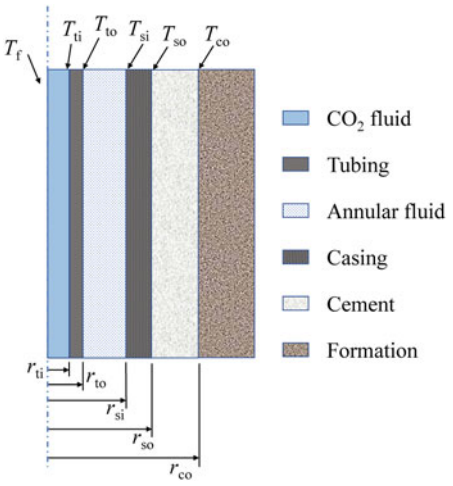

Fig. 44.1 The configuration of the wellbore

$$\frac{\mathrm{d}(\rho_\mathrm{f} v_\mathrm{f})}{\mathrm{d}s} = 0 \tag{44.1a}$$

$$-\frac{\mathrm{d}\left(\rho_\mathrm{f} v_\mathrm{f}^2\right)}{\mathrm{d}s} - \frac{\mathrm{d}p_\mathrm{f}}{\mathrm{d}s} + \rho_\mathrm{f} g \cos\theta - f_\mathrm{w} = 0 \tag{44.1b}$$

$$-\frac{\mathrm{d}}{\mathrm{d}s}\left[\rho_\mathrm{f} v_\mathrm{f}\left(e_\mathrm{f} + \frac{1}{2} v_\mathrm{f}^2\right)\right] - \frac{\mathrm{d}}{\mathrm{d}s}(p_\mathrm{f} v_\mathrm{f}) + \rho_\mathrm{f} g v_\mathrm{f} \cos\theta - v_\mathrm{f} f_\mathrm{w} - q = 0 \tag{44.1c}$$

where p_f and v_f represent the pressure and velocity of the injected fluid respectively, ρ_f and e_f are the fluid's density and specific internal energy respectively, g is the gravitational acceleration, s and θ are the well depth and deviation angle respectively. Equations (44.1a)–(44.1c) are the continuity, momentum and energy conservation equations for fluid flow respectively. f_w in Eq. (44.1b) is the frictional force between the viscous fluid and the tubing wall which is calculated as $f\rho_\mathrm{f} v^2{}_\mathrm{f}/(4r_\mathrm{ti})$, where f is the friction coefficient and r_ti is the inner radius of the tubing [18]. The remained term q denotes the radial heat transfer per unit control volume from the surrounding formation to the injected fluid and is estimated as $q = 2U_\mathrm{tot}(T_\mathrm{f} - T_\mathrm{ei})/r_\mathrm{ti}$. T_f and T_ei are the fluid temperature and the initial temperature of the formation respectively, and U_tot is the overall-heat-transfer coefficient based on the tubing inside area. Many wellbore flow models provide efficient methods to obtain U_tot [18, 19].

It should be noted that none of Eqs. (44.1a)–(44.1c) contains the fluid temperature. We introduce it in the above governing equations through the fluid specific enthalpy $h_\mathrm{f} = e_\mathrm{f} + p_\mathrm{f}/\rho_\mathrm{f}$. The gradient of the fluid specific enthalpy is related to the fluid temperature and pressure as [20]:

$$\frac{\mathrm{d}h_\mathrm{f}}{\mathrm{d}s} = c_{p\mathrm{f}} \frac{\mathrm{d}T_\mathrm{f}}{\mathrm{d}s} - c_{p\mathrm{f}} C_\mathrm{Jf} \frac{\mathrm{d}p_\mathrm{f}}{\mathrm{d}s} \tag{44.2}$$

where $c_{p\mathrm{f}}$ and C_Jf are the fluid specific heat capacity and Joule-Thomson coefficient, respectively. Thermal properties of CO_2 have to be determined to solve Eqs. (44.1a)–(44.1c). This work adopts the Span-Wagner equation of state to calculate fluid properties [15]. Solutions to Eq. (44.1) provide the temperature profile and the concerned temperature difference between the injected fluid and the formation.

44.3 Stress Analysis for the Well Section

Figure 44.2 presents a typical geometry of the well cross section composed of casing-cement-formation. Since wells are often as long as several kilometers, the deformation in the horizontal plane as shown in Fig. 44.2 is much larger than the one along the axial direction. Therefore, we undertake a plane-strain approach to evaluate the stress state in the cement. Here, we focus on the cement behind the non-perforated casing above the injection zone, and consider good and poor cementing conditions

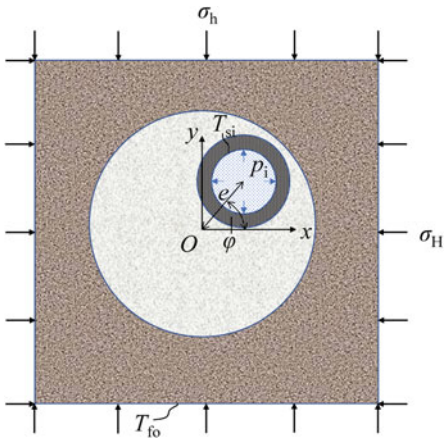

Fig. 44.2 Casing-cement-formation section with boundary conditions and casing eccentricity

corresponding to concentric cemented casing and eccentric cemented casing respectively. The casing eccentricity e is defined as a distance between the centers of the casing and wellbore and the angle φ from the horizontal line to the two centers' connection. The symmetry of geometry and loads restricts that $0 \leq e \leq 1$ and $0 \leq \varphi \leq 90°$. The annular fluid exerts a pressure p_i inside the casing while the well section is subjected to in-situ stresses with $\sigma_H > \sigma_h$. T_{si} and T_{fo} are the temperatures at the inner surface of casing and the formation near the wellbore respectively, which can be determined from the wellbore flow model given in Sect. 44.2.

Under geomechanical loads and temperature fluctuation depicted in Fig. 44.2, stresses would be caused in cement. The stress field can be evaluated by the equilibrium equation and thermoelastic constitutive equation as follows. Neglect the body force, the equilibrium equation is given as [21]:

$$\frac{\partial \sigma_r}{\partial r} + \frac{1}{r}\frac{\partial \tau_{r\theta}}{\partial \theta} + \frac{\sigma_r - \sigma_\theta}{r} = 0 \tag{44.3a}$$

$$\frac{\partial \tau_{r\theta}}{\partial r} + \frac{1}{r}\frac{\partial \sigma_\theta}{\partial \theta} + \frac{2\tau_{r\theta}}{r} = 0 \tag{44.3b}$$

where (r,θ) represents the polar coordinates with the origin at the wellbore center as shown in Fig. 44.2, σ_r, σ_θ and $\tau_{r\theta}$ are the radial, hoop and shear stress components, respectively. It should be noted that the casing is eccentric that breaks the axisymmetric symmetry and introduces θ and $\tau_{r\theta}$ in Eq. (44.3).

For simplicity, we assume the casing, cement and formation are all homogenous, isotropic linear elastic, and then the materials' stress can be expressed in terms of the strain tensor as:

$$\sigma_r = \frac{E}{(1+\nu)(1-2\nu)}[(1-\nu)\varepsilon_r + \nu\varepsilon_\theta - (1+\nu)\alpha(T_c - T_{c0})] \tag{44.4a}$$

$$\sigma_\theta = \frac{E}{(1+\nu)(1-2\nu)}[(1-\nu)\varepsilon_\theta + \nu\varepsilon_r - (1+\nu)\alpha(T_c - T_{c0})] \tag{44.4b}$$

$$\sigma_z = \nu(\sigma_r + \sigma_\theta) - E\alpha(T_c - T_{c0}) \tag{44.4c}$$

$$\tau_{r\theta} = \frac{E}{1+\nu}\varepsilon_{r\theta} \tag{44.4d}$$

where σ_z is the axial stress component, T_c and T_{c0} are the temperature distribution in cement and its initial temperature, respectively, ε_r, ε_θ and $\varepsilon_{r\theta}$ are the radial, hoop and shear strain components respectively. E, ν and α are the materials' Young's modulus, Poisson's ratio and thermal expansion coefficient, respectively. To solve Eq. (44.3), boundary conditions should be provided. From Fig. 44.2, the mechanical boundary conditions are the pressure inside the casing as well as in-situ stresses. Analytical solutions to Eq. (44.3) have been provided for the symmetry situation without a casing eccentricity. However, for asymmetric geometries, it is very difficult to give a solution in close-form. Finite element (FE) methods are convenient to simulate the mechanical response for complex conditions. In this work, the temperature is obtained from the flow model while the stress state is estimated through an FE simulation. Not simultaneously calculating the fluid-structure interaction would reduce computational cost.

44.4 Failure Factors

As aforementioned, the induced stress in cement may cause integrity failure that poses a leakage risk for the stored CO_2. Many researchers and engineers have identified that the primary failure modes of cement include shear compressive failure, radial cracking and interfacial debonding as illustrated in Fig. 44.3. Shear failure occurs when the equivalent stress in the cement is greater than the material's strength. There are many criteria that characterize this kind of failure for cement. Among them, the Mogi-Coulomb criterion is adopted in this work since it has been proven to be applicable to several types of rocks. It defines a shear failure envelope as [22]:

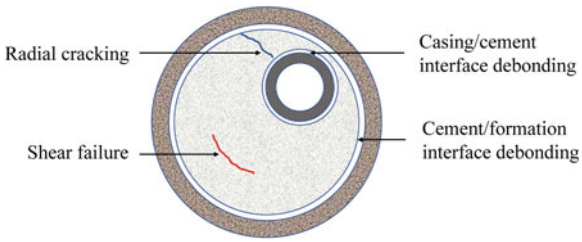

Fig. 44.3 Failure modes of cement for shear failure, radial cracking and interfacial debonding

$$\tau_8 \leq \tau_{\max} \tag{44.5a}$$

$$\tau_8 = \frac{1}{3}\sqrt{(\sigma_1 - \sigma_2)^2 + (\sigma_2 - \sigma_3)^2 + (\sigma_3 - \sigma_1)^2} \tag{44.5b}$$

$$\tau_{\max} = \frac{\sigma_{\mathrm{uc}}(1 - \sin\phi)}{2\cos\phi} + \frac{\sin\phi(\sigma_1 + \sigma_3)}{2} \tag{44.5c}$$

where τ_8 is the octahedral shear stress and $\tau_{\max}$ is the maximum material's allowable shear stress, σ_i ($i = 1, 2, 3$) are the principle stress components in cement, σ_{uc} represents the unconfined compressive strength of cement, and ϕ is the material's internal friction angle. According to Eq. (44.5), the failure factor for shear compressive strength can be defined as:

$$\eta_{\mathrm{s}} = \frac{\tau_{8,\max}}{\tau_{\max}} \tag{44.6}$$

where $\tau_{8,\max}$ is the maximum octahedral shear stress calculated by the FE simulation. $\eta_{\mathrm{s}} \geq 1$ indicates a high risk of shear failure in cement.

When the tensile hoop stress in cement surpasses its tensile strength σ_{t}, radial cracks may generate. Similarly, the failure factor for radial cracking is:

$$\eta_{\mathrm{r}} = \frac{\sigma_{\theta,\max}}{\sigma_{\mathrm{t}}} \tag{44.7}$$

where $\sigma_{\theta,\max}$ is the maximum tensile hoop stress under certain conditions.

The failure factor for interfacial debonding compares the tensile radial stress at the interfaces between the casing and cement or the cement and formation to the interface strength, which is given as:

$$\eta_{\mathrm{sc}} = \frac{\sigma_{r\mathrm{sc},\max}}{\sigma_{\mathrm{sc}}}, \eta_{\mathrm{cf}} = \frac{\sigma_{r\mathrm{cf},\max}}{\sigma_{\mathrm{cf}}} \tag{44.8}$$

where η_{sc} and η_{cf} denote the interfacial failure factors for the casing/cement and cement/formation interfaces respectively, $\sigma_{r\mathrm{sc},\max}$ and $\sigma_{r\mathrm{cf},\max}$ are the maximum tensile radial stresses at the casing/cement interface or the cement/formation interface respectively, and σ_{sc} and σ_{cf} are interfacial strengths of these two interfaces.

Revealing evolutions of the above failure factors with injection operations such as injection temperature and rate could identify the main failure mode during CO_2 injection and provide guidance for maintaining well integrity.

44.5 Wellbore Parameters and Injection Operations

Equation (44.1) provides the temperature of the well structure which could be used to estimate the induced stress in cement and failure factors from an FE simulation. Then the obtained failure factors quantify the impact of CO_2 injection on the well integrity. To concrete our approach, we consider an injection well of CO_2 with typical loading cases. The geometry of the well is listed in Table 44.1. The deviation angle of the well is set to be zero i.e. a vertical well. The surface temperature is 4.5 °C with a temperature gradient of 4.2 °C/100 m. From Eqs. (44.1) and (44.3), thermal and mechanical properties should be supplied to calculate the temperature and stress as presented in Table 44.2. The thermodynamic properties of the injected CO_2 are determined from the Span-Wagner equation of state by iteration in each calculation step.

Previous studies have indicated that the injection temperature and rate have important effects on the temperature profile [14]. Here, we investigate the influence of these two injection parameters on the temperature in the cement above the injection zone and their impact on failure factors. In practice, the CO_2 temperature varies from 25 °C for onshore pipeline transport to −50 °C for offshore pipeline transport. Hence, we consider an injection temperature range of −20 to 20 °C. We fix the annual injection as 1t/a per well and change the injection rate from 1 kg/s to 20 kg/s, and the injection

Table 44.1 Geometry of the well

Parameter	Value
Well depth (m)	2000
Inner radius of tubing (mm)	31.0
Outer radius of tubing (mm)	36.5
Inner radius of casing (mm)	60.68
Outer radius of casing (mm)	69.85
Radius of wellbore (mm)	107.95

Table 44.2 Thermal and mechanical properties of materials

Properties	Tubing/Casing	Cement	Formation	Annular fluid
Thermal conductivity (W/m K)	47	0.72	2	0.6
Specific heat (J/kg K)	/	/	900	4100
Density (kg/m^3)	/	/	2 500	1000
Viscosity (Pa s)	/	/	/	6×10^{-4}
Young's modulus (GPa)	200	1	1	/
Poisson's ratio	0.3	0.23	0.2	/
Thermal expansion coefficient (10^{-6}/°C)	12	10	11	/

time varies accordingly. During injection, the casing inside is subjected to a pressure caused by the annular fluid that can be estimated by the well depth and fluid density. It has been demonstrated that the existence of in-situ stresses would benefit interfacial strength. To study the worst situation, we assume $\sigma_H = \sigma_h = 0$ in our research.

44.6 Results and Discussions

It can be inferred that a larger temperature difference between the barrier materials would cause a greater stress in cement. We firstly discuss the influence of injection operations on this temperature difference, and then we go to cement's failure factors. Figure 44.4 presents the temperature difference between the tubing inside surface and the formation along the well depth with different injection rates (v_{inj}). The injection time (t_{inj}) is also illustrated. Figure 44.4 demonstrates that the maximum temperature difference occurs at the well section just above the injection zone (not including the well section below the packer). In addition, the temperature difference increases with the well depth. With slow injection rates, this increase exhibits a non-linear behavior, while it is nearly a straight line at faster injection rates ($v_{inj} > 5$ kg/s). Faster injection rates would induce a larger temperature difference at deeper positions. It should be noted that as the injection rate increases further, the temperature differences corresponding to variant injection rates are close to each other. For example, $T_{si} - T_e$ is -38.86 °C for $v_{inj} = 5$ kg/s and it is -40.94 °C and -41.75 °C when v_{inj} is 10 kg/s and 20 kg/s, respectively.

To reveal the influence of injection rates on the temperature difference between the casing and formation clearly, Fig. 44.5 plots $T_{si} - T_e$ at the bottom section as a function of the injection rate with different injection temperatures. It is obvious that the temperature difference will reach a steady value as the injection rate becomes faster and faster. At high injection rates, the heat transfer from the surrounding formation to the injected fluid goes quickly. It takes a short time to get the system

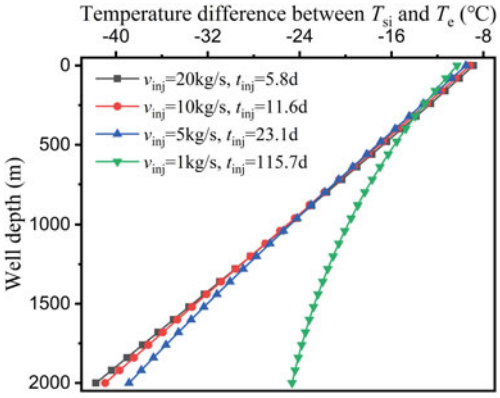

Fig. 44.4 The temperature difference between T_{si} and T_e along the well depth for various injection rates

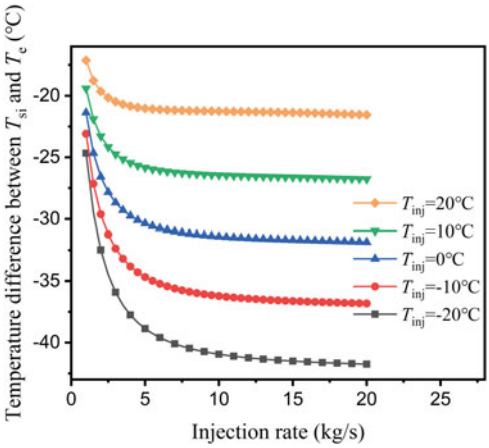

Fig. 44.5 The temperature difference between T_{si} and T_e as a function of the injection rate

to thermal equilibrium. Figure 44.5 also tells that the injection temperature plays an important role in the temperature difference. Specifically, $T_{si}-T_e$ is -21.55 °C for $T_{inj} = 20$ °C while is -41.75 °C for $T_{inj} = -20$ °C, it drops 93.7%.

Our main purpose in this study is to illustrate the effects of injection operations on cement's failure factors defined in Eqs. (44.6)–(44.8). At first, we consider a good cementing quality i.e. $e = 0$. Then we investigate the fluctuation of failure factors with poor cementing. Figure 44.6a and b provide evolutions of failure factors with the injection temperature and rate with a good cementing job, respectively. From Fig. 44.6a, it can be seen that the shear compressive failure factor η_s changes very slowly (from 0.16 to 0.19) as the injection temperature grows from -20 °C to 20 °C (v_{inj} is fixed as 20 kg/s). However, η_r, η_{sc} and η_{cf} all decrease linearly as T_{inj} increases. In particular, η_r changes from 0.934 to 0.797 which is close to 1. η_{sc} is no more than 1 as the injection temperature goes down. The most dangerous situation is that when T_{inj} is below -10 °C, η_{cf} is larger than 1 that means debonding would occur at the cement/formation interface very likely. As the fluid is injected faster (1 kg/s $\leq v_{inj} \leq$ 20 kg/s and T_{inj} is fixed as -20 °C), η_s decreases from 0.186 to 0.162 that is a tiny variation. Similar to Fig. 44.6a, η_r, η_{sc} and η_{cf} go higher and higher when injection rate increases. η_r still changes a little and is near the dangers value. η_{sc} is always smaller than 1, while as v_{inj} goes beyond 3 kg/s η_{cf} becomes greater than 1. For both injection parameters, radial cracking and debonding at the cement/formation interface are more dangerous than the other two failure modes. It needs to be paid more attention to guarantee the bonding strength between the cement and formation when CO_2 is injected at a low temperature and a fast rate.

Previous studies have showed that a casing eccentricity will cause stress concentration in cement, which would rise failure risk for cement integrity. From Fig. 44.6 we can learn that when $T_{inj} = -20$ °C and $v_{inj} = 3$ kg/s, the failure factors for radial cracking and cement/formation interface debonding are 0.896 and 0.966, respectively. Both two failure modes are in a dangerous zone. We estimate failure factors under this injection operation with different casing eccentricities as shown in

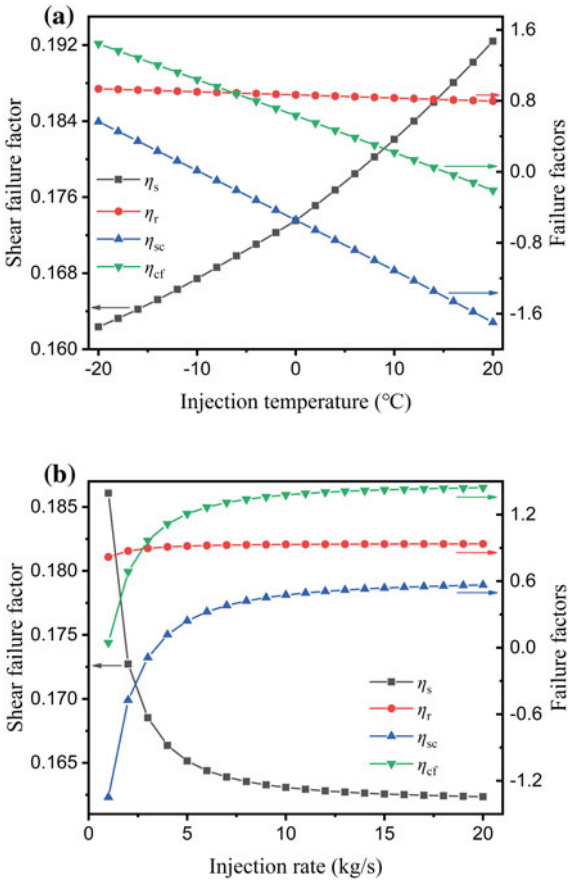

Fig. 44.6 Evolutions of cement's failure factors with injection operations with a good cementing job: **a** injection temperature and **b** injection rate

Fig. 44.7. In general, there is no clear relation between failure factors and the casing eccentricity. For the given injection parameters, η_s is 0.169 with a good cementing quality. Figure 44.7a shows that η_s is safe since its maximum value is 0.186 when $e = 0.99$ and $\varphi = 75°$. For radial cracking, η_r is enlarged to 1.07 when $e = 0.99$ and $\varphi = 45°$. In the range of eccentricity, η_{sc} is negative as shown in Fig. 44.7c. Again, the cement/formation debonding has the highest risk with casing eccentricity that it will increase to 1.20 at $e = 0.99$ and $\varphi = 60°$. It is worth noting that a larger degree of eccentricity would induce a higher η_{cf}. All the above failure factor increases are obtained at $e = 0.99$, which is a very extreme condition. In fact, modern oil and gas industry has made a great progress in drilling and completion, and e is normally no more than 0.25. For this eccentricity degree, when φ varies in the range of [0, 90°], η_{cf} increases by 11.1% at most.

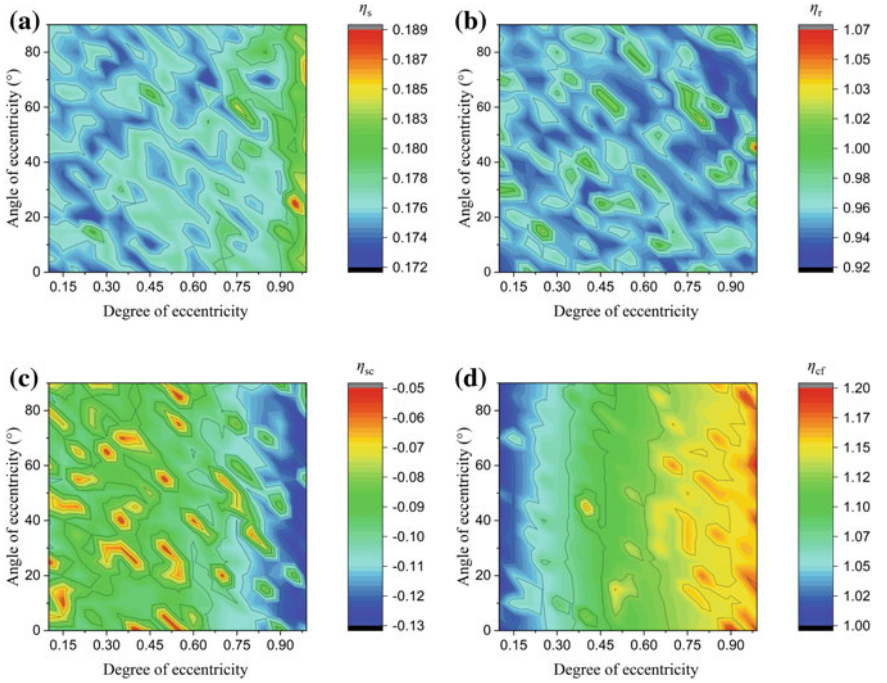

Fig. 44.7 Effects of casing eccentricity on cement's failure factors: **a** shear failure **b** radial cracking **c** casing/cement debonding **d** cement/formation debonding

44.7 Conclusions

In this paper, we present a wellbore flow model to predict the temperature profile along the well depth during CO_2 injection. An FE simulation is carried out to estimate the stress state in cement above the injection zone. To evaluate the cement integrity, we define failure factors for different failure modes including shear compressive failure, radial cracking and interfacial debonding. Then we present effects of the injection temperature, injection rate and casing eccentricity on the defined failure factors. The relevant results show that the temperature difference between the casing inside and formation is higher at deeper positions. Lower injection temperatures and faster injection rates would induce a larger temperature difference. For CO_2 injection wells, radial cracking and cement/formation debonding are the potential failure modes during operation. The shear failure factor will increase with the injection temperature and decrease with the injection rate. The other failure factors would rise at a lower injection temperature and a faster injection rate. Severe casing eccentricities would enlarge failure factors in a large extent and the cement/formation debonding is the most dangerous failure mode due to a poor cementing job.

Acknowledgements This work was supported by the National Key R&D Program of China (Grant No. 2018YFB0605502), the Natural Science Foundation of Beijing (Grant No. 2182062), and the National Natural Science Foundation of China (Grant No. 11872378).

References

1. Haszeldine, R.S.: Carbon capture and storage: how green can black be? Science **325**(5948), 1647–1652 (2009)
2. Vilarrasa, V., Rutqvist, J.: Thermal effects on geologic carbon storage. Earth Sci. Rev. **165**, 245–256 (2017)
3. Carroll, S., Carey, J.W., Dzombak, D., Huerta, N.J., Li, L., Richard, T., Um, W., Walsh, S.D.C., Zhang, L.: Review: role of chemistry, mechanics, and transport on well integrity in CO_2 storage environments. Int. J. Greenh. Gas Control. **49**, 149–160 (2016)
4. Alcalde, J., Flude, S., Wilkinson, M., Johnson, G., Edlmann, K., Bond, C.E., Scott, V., Gilfillan, S.M.V., Ogaya, X., Haszeldine, R.S.: Estimating geological CO_2 storage security to deliver on climate mitigation. Nat. Commun. **9**(1), 2201 (2018)
5. Newell, D.L., Carey, J.W.: Experimental evaluation of wellbore integrity along the cement-rock boundary. Environ. Sci. Technol. **47**(1), 276–282 (2013)
6. Kiran, R., Teodoriu, C., Dadmohammadi, Y., Nygaard, R., Wood, D., Mokhtari, M., Salehi, S.: Identification and evaluation of well integrity and causes of failure of well integrity barriers (a review). J. Nat. Gas Sci. Eng. **45**, 511–526 (2017)
7. Bois, A.-P., Vu, M.-H., Ghabezloo, S., Sulem, J., Garnier, A., Laudet, J.-B.: Cement sheath integrity for CO_2 storage—an integrated perspective. Energy Procedia **37**, 5628–5641 (2013)
8. Shadravan, A., Schubert, J., Amani, M., Teodoriu, C.: Using fatigue-failure envelope for cement-sheath-integrity evaluation. SPE Drill. Complet. **30**(1), 68–75 (2015)
9. Torsæter, M., Todorovic, J., Lavrov, A., Gawel, K., Lund, H., Roy, P., Carroll, S.: Avoiding damage of CO_2 injection wells caused by temperature variations. Energy Procedia **114**, 5275–5286 (2017)
10. Thiercelin, M.J., Dargaud, B., Baret, J.F., Rodriquez, W.J.: Cement design based on cement mechanical response. SPE Drill. Complet. **13**(4), 266–273 (1998)
11. Yu, G., Elliot, T.R., Prevost, J.H.: Effects of thermal stresses on caprock integrity during CO_2 storage. Int. J. Greenh. Gas Control. **12**(1), 300–309 (2013)
12. Nygaard, R., Salehi, S., Weideman, B., Lavoie, R.G.: Effect of dynamic loading on wellbore leakage for the Wabamun area CO_2-sequestration project. J. Can. Pet. Technol. **53**(1), 69–82 (2014)
13. Aursand, P., Hammer, M., Lavrov, A., Lund, H., Munkejord, S.T., Torsæter, M.: Well integrity for CO_2 injection from ships: simulation of the effect of flow and material parameters on thermal stresses. Int. J. Greenh. Gas Control. **62**, 130–141 (2017)
14. Roy, P., Morris, J.P., Walsh, S.D.C., Iyer, J., Carroll, S.: Effect of thermal stress on wellbore integrity during CO_2 injection. Int. J. Greenh. Gas Control. **77**, 14–26 (2018)
15. Li, X., Li, G., Wang, H., Tian, S., Song, X., Lu, P., Wang, M.: A unified model for wellbore flow and heat transfer in pure CO_2 injection for geological sequestration, EOR and fracturing operations. Int. J. Greenh. Gas Control. **57**, 102–115 (2017)
16. Ruan, B., Xu, R.X., Ouyang, X., Luo, F., Jiang, P.: Flow and thermal modeling of CO_2 in injection well during geological sequestration. Int. J. Greenh. Gas Control. **19**, 271–280 (2013)
17. White, F.M.: Fluid Mechanics, 7th edn. McGraw-Hill, New York (2009)
18. Pan, L., Oldenburg, C.M., Wu, Y.S., Pruess, K.: Wellbore flow model for carbon dioxide and brine. Energy Procedia **1**(1), 71–78 (2009)
19. Hasan, A.R., Kabir, C.S.: Wellbore heat-transfer modeling and applications. J. Petrol. Sci. Eng. **86–87**(3), 127–136 (2012)

20. Alves, I.N., Alhanati, F.J.S., Shoham, O.: A Unified model for predicting flowing temperature distribution in wellbores and pipelines. SPE Prod. Eng. **7**(4), 363–367 (1992)
21. Sadd, M.H.: Elasticity: Theory, Applications, and Numerics, 2nd edn. Academic Press, Burlington (2009)
22. Andrade, J.D., Sangesland, S.: Cement sheath failure mechanisms: numerical estimates to design for long-term well integrity. J. Petrol. Sci. Eng. **147**, 682–698 (2016)